Impact shock origin of diamonds in ureilite meteorites

Fabrizio Nestola[a,b,1], Cyrena A. Goodrich[c,1], Marta Morana[d], Anna Barbaro[d], Ryan S. Jakubek[e], Oliver Christ[a], Frank E. Brenker[b], M. Chiara Domeneghetti[d], M. Chiara Dalconi[a], Matteo Alvaro[d], Anna M. Fioretti[f], Konstantin D. Litasov[g], Marc D. Fries[h], Matteo Leoni[i,j], Nicola P. M. Casati[k], Peter Jenniskens[l], and Muawia H. Shaddad[m]

[a]Department of Geosciences, University of Padova, I-35131 Padova, Italy; [b]Geoscience Institute, Goethe University Frankfurt, 60323 Frankfurt, Germany; [c]Lunar and Planetary Institute, Universities Space Research Association, Houston, TX 77058; [d]Department of Earth and Environmental Sciences, University of Pavia, I-27100 Pavia, Italy; [e]Astromaterials Research and Exploration Science Division, Jacobs Johnson Space Center Engineering, Technology and Science, NASA, Houston, TX 77058; [f]Institute of Geosciences and Earth Resources, National Research Council, I-35131 Padova, Italy; [g]Vereshchagin Institute for High Pressure Physics RAS, Troitsk, 108840 Moscow, Russia; [h]NASA Astromaterials Acquisition and Curation Office, Johnson Space Center, NASA, Houston, TX 77058; [i]Department of Civil, Environmental and Mechanical Engineering, University of Trento, I-38123 Trento, Italy; [j]Saudi Aramco R&D Center, 31311 Dhahran, Saudi Arabia; [k]Swiss Light Source, Paul Scherrer Institut, 5232 Villigen, Switzerland; [l]Carl Sagan Center, SETI Institute, Mountain View, CA 94043; and [m]Department of Physics and Astronomy, University of Khartoum, 11111 Khartoum, Sudan

Edited by Mark Thiemens, University of California San Diego, La Jolla, CA, and approved August 12, 2020 (received for review October 31, 2019)

The origin of diamonds in ureilite meteorites is a timely topic in planetary geology as recent studies have proposed their formation at static pressures >20 GPa in a large planetary body, like diamonds formed deep within Earth's mantle. We investigated fragments of three diamond-bearing ureilites (two from the Almahata Sitta polymict ureilite and one from the NWA 7983 main group ureilite). In NWA 7983 we found an intimate association of large monocrystalline diamonds (up to at least 100 μm), nanodiamonds, nanographite, and nanometric grains of metallic iron, cohenite, troilite, and likely schreibersite. The diamonds show a striking texture pseudomorphing inferred original graphite laths. The silicates in NWA 7983 record a high degree of shock metamorphism. The coexistence of large monocrystalline diamonds and nanodiamonds in a highly shocked ureilite can be explained by catalyzed transformation from graphite during an impact shock event characterized by peak pressures possibly as low as 15 GPa for relatively long duration (on the order of 4 to 5 s). The formation of "large" (as opposed to nano) diamond crystals could have been enhanced by the catalytic effect of metallic Fe-Ni-C liquid coexisting with graphite during this shock event. We found no evidence that formation of micrometer(s)-sized diamonds or associated Fe-S-P phases in ureilites require high static pressures and long growth times, which makes it unlikely that any of the diamonds in ureilites formed in bodies as large as Mars or Mercury.

diamond | impact shock | ureilitic diamonds | ureilites | carbon phases

The origin of diamonds in ureilite meteorites is a highly controversial topic among planetary geologists with three main hypotheses being debated: 1) formation by impact shock conversion from graphite (1–7), 2) formation at low pressure in the solar nebula by chemical vapor deposition (8–10), and 3) formation at high static pressures in a planetary-sized body (11–13).

The ureilites form the second largest group of achondrites. They are ultramafic rocks mainly composed of olivine and pyroxene, with interstitial carbon, metal, and sulfide phases (14–19). They represent the mantle of a partially differentiated parent body (the ureilite parent body, or UPB) that experienced igneous processing at temperatures up to 1,200 to 1,300 °C (18). The UPB was catastrophically disrupted by a major impact before it had completely cooled, with ureilites being derived from daughter bodies that reassembled in the aftermath of the disruption (17, 19–21).

Carbon abundances are notably high in ureilites, ranging up to 8.5 wt % (19, 22), with the carbon occurring principally as graphite (18). In ureilites of very low shock level (based on shock indicators in the silicates), the graphite occurs as millimeter-sized euhedral (blade-shaped or tabular) crystals showing prominent (0001) cleavage, closely associated with Fe, Ni metal, and sulfides (23, 24) (*SI Appendix*, Fig. S1). Diamonds have not been reported in the lowest-shock samples (2, 25). Most ureilites, however, are shocked to various degrees and in these samples the graphite areas, though still having external blade-shaped morphologies, are internally polycrystalline (18). Diamonds and lonsdaleite [diamond with stacking faults and twinning defects (26)] occur embedded in these areas, constituting a volumetrically minor (thus disproportionately illustrious) component of ureilites.

Although the presence of diamonds in these meteorites was reported more than a century ago, the process by which the diamonds formed has been hotly debated and is still controversial. The first hypothesis on the origin of diamond in ureilites dates back to 1956, when Urey (11) proposed that diamonds may form under static high-pressure conditions in the interior of large meteorite parent bodies. A few years later, in his seminal work on diamonds from the Goalpara and Novo Urei ureilites, Lipschutz (1) proposed that diamonds in ureilites were formed by shock conversion of graphite, a hypothesis that has been supported by many subsequent studies (2–7). A third hypothesis that has been discussed is that diamonds in ureilites formed at low pressure in the solar nebula by chemical vapor deposition (8–10).

Significance

The origin of diamonds in ureilites is still a debated issue among the scientific community, with significant implications for the sizes of early Solar System bodies. We investigated three diamond-bearing ureilites by a multimethodological approach using scanning electron microscopy, micro X-ray diffraction, transmission electron microscopy, and micro-Raman spectroscopy, with the aim of determining the origin of the diamonds. Our results show that formation of both microdiamonds and nanodiamonds in ureilites can be explained by impact shock events on a small planetesimal and does not require long growth times at high static pressures within a Mercury- or Mars-sized body.

Author contributions: F.N. and C.A.G. designed research; F.N., C.A.G., M.M., A.B., O.C., F.E.B., A.M.F., and N.P.M.C. performed research; R.S.J., F.E.B., and M.D.F. contributed new reagents/analytic tools; F.N., C.A.G., M.M., A.B., O.C., M.C. Domeneghetti, M.C. Dalconi, M.A., A.M.F., M.L., and N.P.M.C. analyzed data; and F.N., C.A.G., M.M., A.B., R.S.J., O.C., F.E.B., M.C. Domeneghetti, M.C. Dalconi, M.A., A.M.F., K.D.L., M.D.F., M.L., N.P.M.C., P.J., and M.H.S. wrote the paper.

The authors declare no competing interest.

This article is a PNAS Direct Submission.

[1]To whom correspondence may be addressed. Email: fabrizio.nestola@unipd.it or goodrich@lpi.usra.edu.

This article contains supporting information online at https://www.pnas.org/lookup/suppl/doi:10.1073/pnas.1919067117/-/DCSupplemental.

First published September 28, 2020.

Recent work on the Almahata Sitta (AhS) polymict ureilite (12, 13) reported the presence of large diamonds (with inclusions of chromite and Fe-S-P phases) in a ureilitic clast and suggested that such diamonds could only be formed at static pressures higher than 20 GPa. This would imply either that the UPB was similar in size to Mercury or Mars (13), or that diamonds in ureilites are exogenous to the UPB (27).

In order to provide insight into the origin of diamonds in ureilites, we investigated carbon phases in two ureilitic stones from AhS, samples AhS 209b and AhS 72, and also the NWA 7983 main group ureilite (28), by single-crystal micro X-ray diffraction (XRD) both in-house at the University of Padova (all three samples) and using synchrotron radiation at Paul Scherrer Institute, Villigen, Switzerland (AhS samples only). In addition, micro-Raman spectroscopy was performed on several carbon areas in NWA 7983 at ARES (Astromaterials Research and Exploration Science), Johnson Space Center, NASA, Houston, TX. Our results cast reasonable doubt on purported evidence for formation of ureilitic diamonds under high static pressures and provide strong evidence for their formation by impact shock at pressure peaks possibly as low as 15 GPa.

Results

Samples. AhS 209b and 72 are two stones from the AhS meteorite, which fell in the Nubian desert in 2008 (19, 29–31). They are fine-grained, porous ureilites showing various degrees of "impact smelting" and shock metamorphism as previously described for fine-grained AhS ureilites and a few main group ureilites (32, 33). Olivine areas in AhS 209b are completely mosaicized (*SI Appendix*, Fig. S2). They consist of aggregates of ∼5- to 20-μm-sized equigranular tiles (adopting the terminology of ref. 32) with tiny amounts of interstitial pyroxene and Si+Al-rich glass, which are inferred to represent recrystallized versions of originally ∼0.5- to 1-mm-sized primary grains (e.g., refs. 32 and 33). The olivine largely preserves a typical ureilite olivine core composition of Fo ∼79, except in reduction rims near inferred original grain boundaries and/or carbon areas. Reduction rim compositions range up to Fo ∼93. Pigeonitic pyroxene areas in AhS 209b also show complete mosaicism with extensive in situ reduction and porosity. They consist of aggregates of ∼5- to 10-μm-sized subhedral to anhedral grains, with varying amounts of interstitial Ca-enriched pyroxenes and Si-Al–enriched glass. Pores and small grains of metal and sulfide among the pyroxene grains are common. The pyroxene tiles show reverse zoning. Cores are reduced (core Mg#s up to ∼93) relative to inferred primary compositions (∼Mg# 81, such as would have been in equilibrium with Fo ∼79 olivine in a typical lower-shock ureilite) with varying Wo contents (∼2 to 8). Pyroxene textures such as these were described by Warren and Rubin (32) in several main group and AhS ureilites and attributed to "impact smelting" (concomitant melting and chemical reduction by carbon) of originally larger primary pigeonite grains. Elongated masses of carbon phases and metal grains are dispersed throughout the sample, commonly occurring along inferred primary silicate grain boundaries (Fig. 1 *A* and *B* and *SI Appendix*, Fig. S3).

The fragment of AhS 72 that we examined is dominated by olivine and shows a higher degree of shock metamorphism than 209b. Olivine is completely recrystallized to ∼1- to 20-μm-sized equigranular (anhedral to subhedral) grains in a groundmass (of varying proportions relative to the amount of olivine) of pyroxene. The olivine grains are highly reduced (Fo ∼99) and nearly free of inclusions, suggesting recrystallization from a melt (or at least at very high temperatures) under highly reducing conditions. Interstitial pyroxene compositions range from Wo 0.8 to Wo 34 and are also reduced (Mg# 88 to 99). Pores, masses of carbon phases (∼20 to hundreds of micrometers), and grains of metal are abundant throughout the section.

The NWA 7983 meteorite was found in 2013 in Morocco. The stone has a total mass of 424.3 g and was classified as a main group ureilite (28). The original description noted that the meteorite was extremely resistant to cutting and polishing and suggested that diamond was abundant (28), and our work confirms this. We studied four polished sections of NWA 7983. A polished thick section with an area of about 2 cm^2 was used for scanning electron microscopy (SEM) observations (not carbon-coated; see *SI Appendix*, sections 1.1 and 1.2) followed by micro XRD. Three polished thin sections were used for optical microscopy and additional SEM observations (both carbon-coated and not carbon-coated). NWA 7983 consists mainly of olivine, minor pyroxene, and ∼6 vol % masses of carbon phases. Metal, Fe-oxides/hydroxides (presumed terrestrial replacements of metal), troilite, and Cr-rich sulfides occur cross-cutting silicates and as blebs. The olivine shows a high degree of shock metamorphism, with textures similar to those in AhS 72 (*SI Appendix*, Fig. S4). All olivine areas are either mosaicized with ∼2- to 12-μm-sized euhedral tiles and very minor interstitial feldspathic material, or recrystallized to ∼1- to 20-μm-sized equigranular (anhedral to subhedral) grains in a groundmass of minor pyroxene. The degree of reduction of the olivine varies greatly. Some areas (inferred original grains) are dominantly Fo 82 to 83, which may be close to the primary composition, while others are strongly reduced with Fo ∼90 to 98. The interstitial pyroxenes vary in Wo from ∼2 to 33 and Mg# ∼84 to 92. Elongated masses of carbon phases, as well as metal ± sulfide grains (wholly or partly altered to terrestrial Fe-hydroxides), are dispersed throughout the sample. Similar to AhS 72, the degree of recrystallization of the silicates is so high that the outlines of primary silicate grain boundaries are difficult to discern.

The carbon masses typically occur as elongated (blade-shaped), internally layered structures of up to 1 mm in length and 300 μm in width (Fig. 1 *C–E* and *SI Appendix*, Figs. S5 and S6). In one of the sections that we studied, such blades form a nearly continuous vein ∼1 cm long. In reflected light, the carbon masses contain elongated, highly reflective, high-relief stripes that are parallel to the external morphology of the carbon mass in the long dimension and are inferred to be diamond, based on their optical properties and fluorescence under an electron beam (Fig. 1*D* and *SI Appendix*, Figs. S5 *A–C* and S6*A*). Some of these contain structures that resemble {111} crystal faces of octahedral diamonds. In back-scattered electron images (BEI), the carbon masses also show a striped appearance (parallel to the external morphology of the carbon mass), which is defined by light and dark areas (Fig. 1*C* and *SI Appendix*, Figs. S5 *D* and *E* and S6*B*). The lighter areas contain numerous tiny, bright grains of what appears to be metallic Fe and Fe-sulfides, based on energy-dispersive X-ray spectroscopy (EDS) spectra showing peaks for C, Fe, and S. The darker areas appear to be largely free of inclusions and have EDS spectra showing only C. Based on fluorescence under the electron beam, diamonds are abundant in both the light and the dark areas. In general, the high-reflectance, high-relief areas observed in reflected light correspond closely to the darker areas in BEI (Fig. 1 *C* and *D* and *SI Appendix*, Fig. S6 *A* and *B*).

None of the samples studied in this work shows any high-pressure polymorphs of olivine such as wadsleyite and ringwoodite, even in veins or fractures where we specifically searched for them by micro-Raman spectroscopy.

Micro XRD. Using reflected light and/or back-scattered electron images of thick sections that were not carbon-coated we located carbon areas for micro XRD in the three samples. We gently removed portions of such carbon areas (*SI Appendix*, section 1.3) and analyzed them by micro XRD.

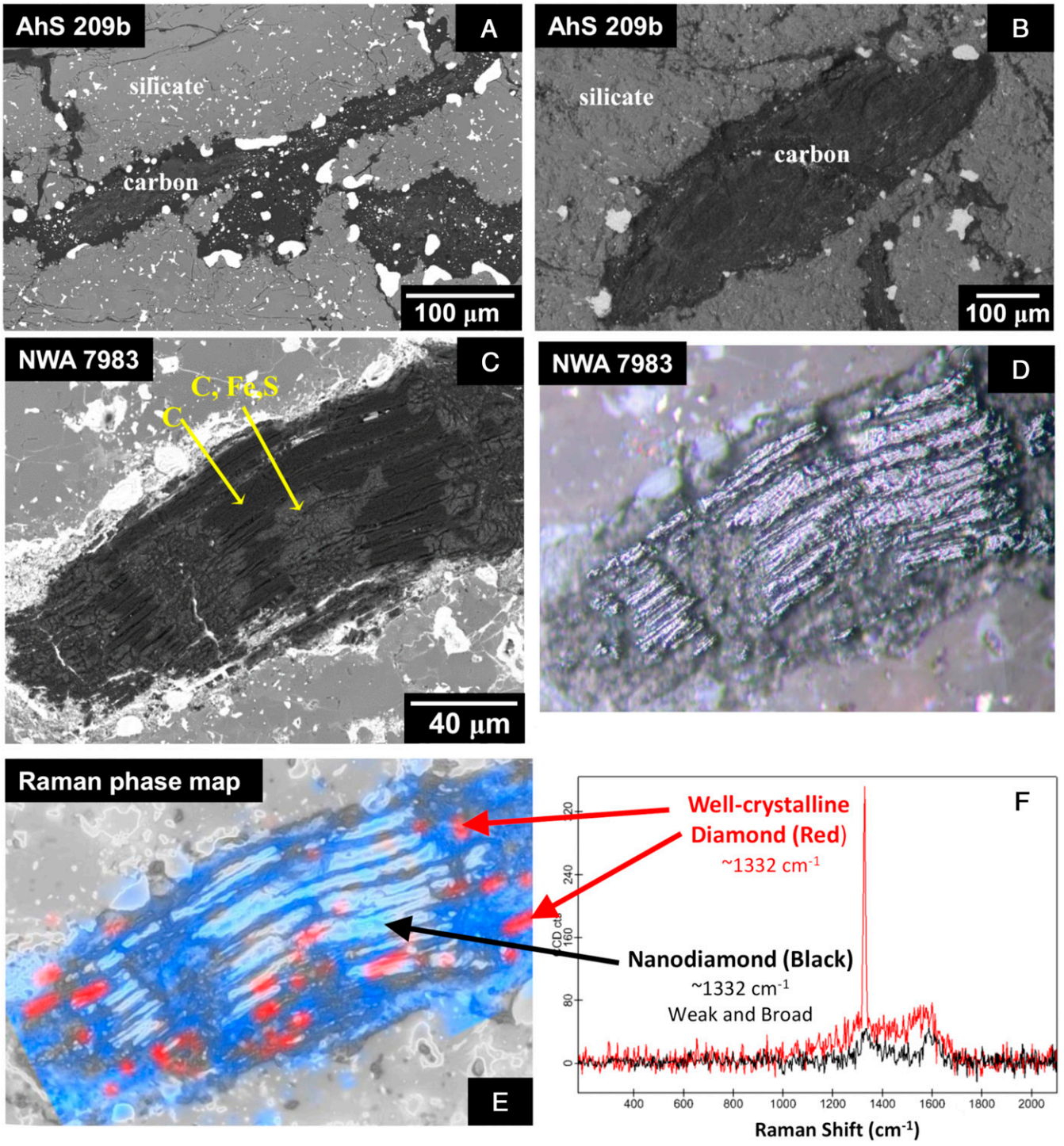

Fig. 1. Carbon masses in polished sections of AhS 209b and NWA 7983. (*A*) BEI of AhS 209b, showing elongated masses of carbon phases located along inferred primary silicate grain boundaries (see also *SI Appendix*, Fig. S3 for a lower-magnification view). (*B*) BEI of non-carbon-coated section of AhS 209b in low-vacuum mode (hence low contrast). BEI of other carbon areas in AhS 209b are shown in *SI Appendix*, Fig. S3. (*C*) BEI of carbon-coated section of NWA 7983 in high-vacuum mode. Carbon masses in this sample tend to have elongated, blade-like morphology and internally show a structure of dark and light stripes parallel to the long edges of the carbon mass (see also *SI Appendix*, Fig. S4). Dark areas show only C, whereas lighter areas show C, Fe, and S peaks in EDS spectra. (*D*) Reflected light image of same area as in *C*. Highly reflective, high-relief stripes correlate with dark areas in BEI and are inferred to be diamond from their optical properties, as well as fluorescence under the electron beam. (*E*) Raman phase map of area in *C* and *D*. The intensity of the red color corresponds to the intensity of the diamond ~1,332-cm^{-1} band. The intensity of the blue color corresponds to the intensity of the graphite G band (~1,575 cm^{-1}). In nanodiamonds, the ~1,332-cm^{-1} band is broad, has low intensity, and is downshifted, making it difficult to detect. Thus, the Raman image is predominantly sensitive to large diamonds (red) while most nanodiamonds likely go undetected (38, 39). In this Raman image, nanodiamonds were detected only in a few areas, although XRD results indicate that they are present throughout the carbon mass. (*F*) Raman spectra of large diamonds (red) and nanodiamonds (black) from *E*.

AhS 72 and AhS 209b. The sections of carbon materials removed from the AhS 209b and AhS 72 samples were two irregularly shaped grains of 320 μm and 380 μm, respectively, along their longest dimension (*SI Appendix*, Fig. S7). Synchrotron radiation micro XRD showed that these two fragments are both composed mainly of diamonds, graphite and metallic iron (minor troilite was also detected; see *SI Appendix*, section 1.4). Fig. 2*A* shows the X-ray diffractogram and the diffraction image of the AhS 209b fragment. As demonstrated by the diffraction rings (rather than individual diffraction spots), the sample is polycrystalline. A similar observation was made for the AhS 72 sample (the diffractogram and diffraction images for AhS 72 are shown in *SI Appendix*, Fig. S8). Diffraction line profile analysis (34) using the High Score Plus software package (Panalytical) was applied to estimate the crystallite size of the carbon phases (*SI Appendix*, section 1.4). The results of this analysis are given in *SI Appendix*, Table S1 and show that diamonds in both AhS 209b and AhS 72 are nanometric with crystal size of 17 to 19 nm for AhS 209b and 18 to 25 nm for AhS 72. However, both of the AhS samples show a typical feature of diamond stacking faults (see the shoulder of the 2.06 Å peak of diamond in Fig. 2*A*, more evident in the magnification in *SI Appendix*, Fig. S9) and in order to take into account any defects in diamond and eventually graphite (which shows a significant peak asymmetry and broadening) not considered in the previous profile analysis, we performed a further profile analysis by using DIFFaX+ software (35) (*SI Appendix*, sections 1.4 and 1.5 and Fig. S10) which provides more reliable results for defect-bearing powder materials. This revealed that the samples are characterized by two diamond domain sizes: Smaller domains are on average 3 to 12 nm, whereas the larger ones are larger than 50 nm; for sizes >100 nm, diffraction is no longer reliable for the determination of size and defects in materials. The average graphite crystal size was estimated to be 20 nm. These analyses indicate that in the AhS ureilite fragments studied here diamonds are nanometric with an average size of about 25 nm.

NWA 7983. The BEI observations described above revealed that the carbon masses in NWA 7983 show distinct internal stripes of dark and light areas (Fig. 1 *C* and *D* and *SI Appendix*, Figs. S5 and S6), correlating with stripes of high reflectance and high relief and low reflectance and low relief (respectively) in reflected light. We removed fragments from both dark and light areas within five different carbon masses and investigated them by micro XRD in-house (*SI Appendix*, section 1.5 and S11). The XRD images of dark areas in several of the carbon masses (e.g., Fig. 2) showed no evidence of diffraction rings but only diffraction spots typical of monocrystals. Based on the sizes of the removed fragments, the monocrystals that we investigated ranged from ∼20 to at least 100 μm in size (longest dimensions). The diffraction image for the largest monocrystal that we observed is shown in Fig. 2*B* (BEI and reflected light images of this carbon mass, indicating the area removed and analyzed, are given in *SI Appendix*, Fig. S12). The unit-cell edge length that we determined for this crystal is $a = 3.569$ Å (*SI Appendix*, Table S1), typical of cubic diamond. The absence of evidence for any other phases in the diffractogram of this crystal (or similar ones that we analyzed) is consistent with the observations from EDS analyses in the SEM that only C was detected in dark areas of the carbon masses in this sample. In other fragments removed from dark areas, the diffractograms showed the simultaneous presence of diffraction spots (indicating single crystal diamonds) and diffraction rings (e.g., *SI Appendix*, Fig. S13), indicating that in some of the darker areas large diamond monocrystals are intimately intermixed with nanodiamonds on a scale below that detectable in reflected light or BEI imaging.

The diffraction results for fragments removed from the lighter carbon areas (as seen in BEI) in NWA 7983 yielded results very similar to those obtained on the AhS ureilite fragments. Fig. 2*C* shows that such areas are polycrystalline and mainly composed of diamond, graphite, cohenite (ideally Fe_3C), troilite, and minor metallic iron, consistent with EDS spectra showing the presence of Fe and S in addition to C in such areas. The small shoulder at higher *d*-spacing (e.g., 2.18 Å) with respect to the main peak of diamond at 2.06 Å is characteristic of lonsdaleite as already observed for the AhS 209b and AhS 72 samples. The profile analysis for polycrystalline diamonds in both the light areas and the dark areas indicates that the polycrystalline diamond is nanometric and even smaller than diamonds in the AhS fragments with a size of 9 nm (*SI Appendix*, Table S1). Although it was not possible to model the diffraction peaks of graphite, based on the peak broadening of its most intense peak it is likely that the graphite is also nanometric.

In this study an intimate association of micro- and nanodiamonds has been reported in natural samples, either terrestrial or extraterrestrial. Unfortunately, it was not possible to distinguish microdiamonds from nanodiamonds in either reflected light or BEI, and so our principal method of locating microdiamonds was a "hit-or-miss" approach of removing fragments from sections and X-raying them. This approach was time-consuming, thus limiting the number of areas that could be studied, and resulted in loss of textural context of the diamonds. In order to get an idea of the distribution, shapes, and relative abundance of microdiamonds in situ, we used micro-Raman imaging on several areas using 488-nm excitation (Fig. 1 *E* and *F* and *SI Appendix*, Fig. S6 *C–E*). Raman mapping of these areas easily identifies larger diamond grains [>∼45 nm (36)] from the narrow, high intensity band at ∼1,332 cm^{-1} (37), although it does not allow definitive determination of their sizes (38). These Raman maps show clearly that in a number of places the large diamond grains are elongated along the direction of the stripes seen in BEI and reflected light (parallel to external morphology of the carbon mass) and (as shown particularly in *SI Appendix*, Fig. S6) are concentrated along the stripes, that is, forming stripes of their own. We note that nanodiamonds are not easily identified in Raman spectra (38, 39) and so the Raman images (Fig. 1 *E* and *F*) are less useful for showing their distribution. Nevertheless, the XRD analyses showed clearly that nanodiamonds are present in both light and dark areas of the carbon masses.

Transmission Electron Microscopy. The same fragments of AhS 209b and AhS 72 investigated by XRD were analyzed by transmission electron microscopy (TEM) with the main goal being to verify the crystallite size compared with the results from synchrotron micro XRD. The presence of diamond stacking faults (lonsdaleite), as predicted by micro XRD showing the typical shoulders at higher *d*-spacing with respect to the 2.06 Å peak of diamond (*SI Appendix*, Fig. S9), was confirmed by TEM.

Sections of AhS 72 and AhS 209b suitable for TEM analyses were prepared by focused ion beam and investigated by a Philips 200 CM transmission electron microscope (*SI Appendix*, section 1.6). A typical bright-field image of the AhS 72 sample (Fig. 3, *Left*) shows diamond domains with size between about 20 and 150 nm. At the same time, electron diffraction images (Fig. 3, *Right*) indicate that nanodiamonds are associated with graphite (see the ring at about 3.35 Å) and lonsdaleite (see ring at about 2.18 Å), confirming the XRD results. In addition to these main phases, TEM analyses of the AhS 72 sample also revealed the presence of nanometric metallic iron (evident by XRD) and other phases including cohenite Fe_3C, iron sulphide, and Fe-Ni-P compounds. By XRD we determined the iron sulphide to be troilite, but unfortunately due to the extremely small crystal size between 50 and 100 nm we were unable to determine the identity or stoichiometry of the Fe-Ni-P compounds, which could for example be schreibersite $(Fe,Ni)P_3$. Due to the nanometric

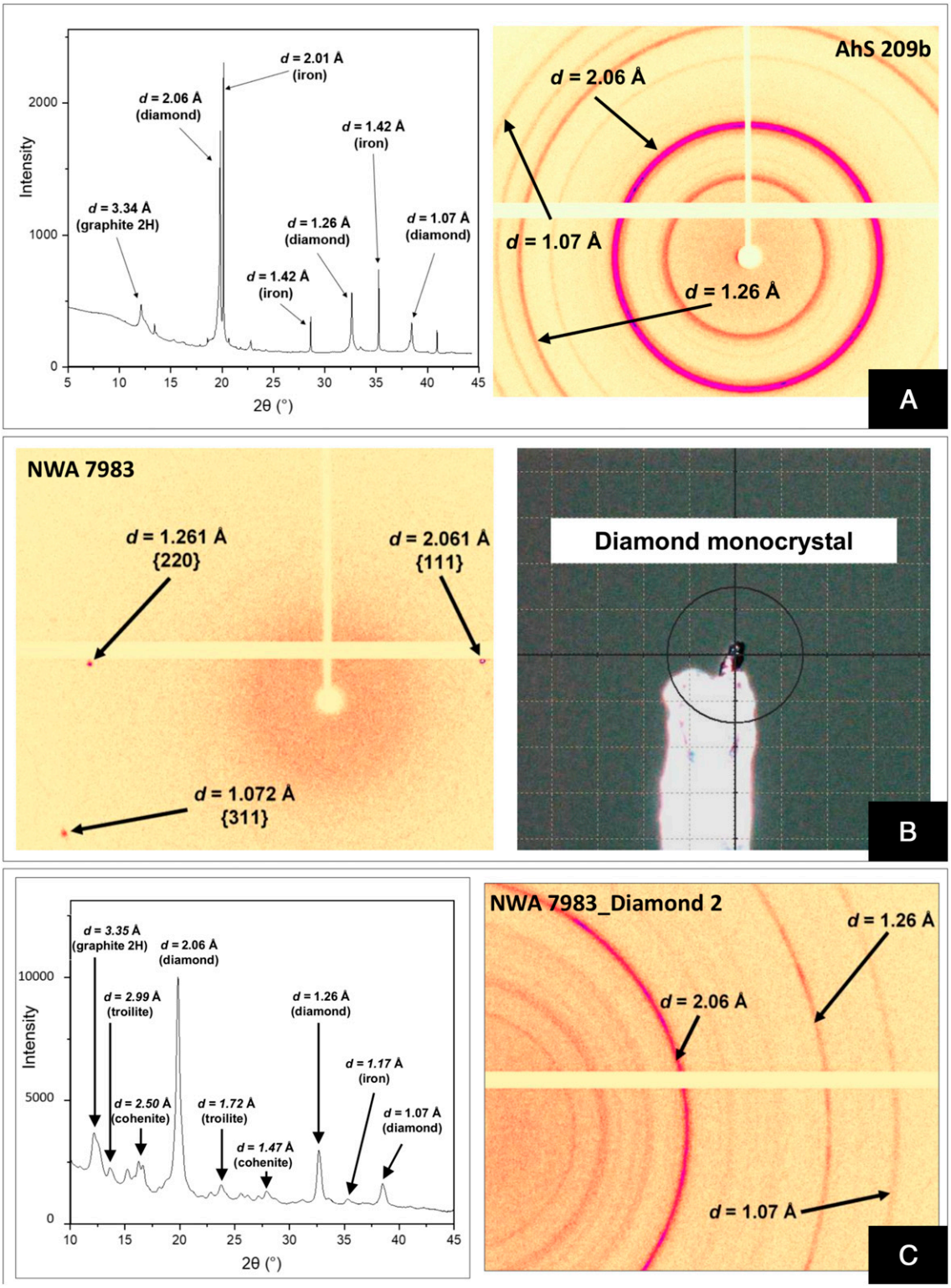

Fig. 2. (*A*) The diffractogram (*Left*) and the diffraction image (*Right*) of the AhS 209b sample, analyzed by micro X-ray powder diffraction at the Paul Scherrer Institute, Villigen, Switzerland. In the diffractogram the most abundant phases found in the carbon-bearing aggregate, polycrystalline diamond, graphite, and iron metal are shown. (*B*) Diffraction image (*Left*) for a fragment of a carbon area in NWA 7983 (from an area that was dark in BEI), showing only diffraction spots typical of a monocrystalline diamond. This monocrystal must be at least 100 μm (the size of the whole fragment removed along its longest dimension). We determined its unit-cell edge length, a = 3.569 Å, typical of diamond. (*C*) Diffractogram (*Left*) and the diffraction image (*Right*) of another fragment of NWA 7983, this one from an area that was lighter in BEI. This sample was analyzed by the Rigaku-Oxford Diffraction Supernova kappa-geometry goniometer at the Department of Geoscience, University of Padova. In this fragment polycrystalline diamond, graphite, iron, cohenite, and a minor abundance of troilite are detected.

size of the diamonds in this sample, we cannot state definitively whether these other phases are inclusions in diamonds or just coexist with diamonds in the carbon masses.

Discussion

AhS 72 and AhS 209b. The results from synchrotron diffraction and TEM analyses of the AhS ureilites studied in this work show nanodiamonds associated with nanographite. In addition, they show metallic iron, troilite, cohenite, and nanometric grains of Fe-Ni-P (likely schreibersite) associated with the diamond phases. The diamond–metal–sulfide–carbide–phosphide association in these AhS stones is the same phase assemblage as that reported in AhS stone MS-170 (13), which argues that the diamond had a common origin in all three stones. However, AhS 72 and AhS 209b are highly shocked ureilites, based on shock features in their silicates (complete mosaicism of olivine). This strongly suggests that the diamonds formed as a result of the same shock event that affected the silicates.

The association of metal, sulfide, carbide, and phosphide phases with diamonds in AhS 72 and AhS 209b is especially significant because Nabiei et al. (13) argued that these phases were definitive evidence of diamond formation at ≥21 GPa static pressure within a parent body with size comparable to Mercury or Mars. Nabiei et al. (13) base this interpretation on the measured molar (Fe+Ni)/(S+P) ratios of the bulk composition of multiphase (metal–sulfide–phosphide) inclusions in diamond, which were close to 3:1. They argue that this implies that the inclusions were trapped as crystals of the phase $(Fe,Ni)_3(S,P)$, which (for $P/[P+S] < 0.2$) is only stable at pressures above 21 GPa. However, this argument is flawed, because at temperatures above 1,275 °C (or lower if S is present) the $(Fe,Ni)_3(S,P)$ phase melts (40, 41). This temperature is almost certainly much lower than temperatures in a Mars-sized body 4.55 Ga ago at depths equivalent to 21 GPa (42). This means either that the interpretation that the inclusions were trapped as $(Fe,Ni)_3(S,P)$ solids is incorrect and their apparent stoichiometry is only a coincidence, or that the proposed formation in a Mars-sized body is incorrect, or both. In fact, the $(Fe,Ni)_3(P,S)$ phase can be formed simultaneously with diamonds by shock compression and quenching, as in shock melt veins in IIE iron meteorite Elga (43). Therefore, the presence of these inclusions does not in any way require a static pressure (large parent body) origin.

With respect to AhS 209b and AhS 72, based on the highly shocked nature of the silicates, and the association of nanodiamond, lonsdaleite, and nanographite, we argue that diamonds in these two ureilites most likely formed by a shock event (44–46) with a peak pressure possibly as low as 15 GPa, based on mosaicism of olivine (47). The presence of the same phase assemblage (diamond–metal–sulfide–carbide–phosphide) in AhS stone MS-170 (13) as in the highly shocked AhS stones studied here strongly suggests that diamond had a common origin in all three samples. However, based on these samples alone, it cannot be ruled out that preexisting, large, defect-poor diamonds [formed, e.g., at high static pressures (12,13)] were reduced in grain size and acquired stacking faults during the shock event that affected the silicates, and that in MS-170 some of these preexisting diamonds happened to survive. Nevertheless, additional evidence provided by NWA 7983 (discussed below) leads to the conclusion that this possibility would be extremely unlikely.

NWA 7983. NWA 7983 is a crucial sample for understanding the origin of diamonds in ureilites because its silicates record a high degree of shock (again, complete mosaicism of olivine) and yet it contains large diamonds (i.e., single crystal diamonds up to at least 100 μm in size) in addition to the nanodiamonds that are accepted to be a common product of shock (44–46). This discovery suggests the possibility that the large diamonds in this ureilite were also formed by the shock process, rather than simply having fortuitously survived it.

A first-order argument supporting this interpretation is the predominantly blade-shaped morphology of the carbon masses in which the diamonds are embedded along with graphite (Fig. 1 and *SI Appendix*, Fig. S5). This external morphology of the carbon areas is the same as that of millimeter-sized euhedral laminate (or tabular) graphite crystals that occur in very-low-shock-level ureilites (*SI Appendix*, Fig. S1) and have been argued to represent the primary form of carbon in all ureilites (23, 24). If the diamonds in NWA 7983 were only remnants of larger diamonds that had formed at high static pressures during long residence times in a planetary mantle, the external shapes of the carbon areas would not be those of graphite crystals (even if graphite laths had been the precursor material) but would be those of typical diamonds formed deep within the Earth's mantle (48). Instead, their shapes, and the prominent striped texture (Fig. 1 and *SI Appendix*, Figs. S5 and S6) of both the nanodiamond aggregates and the larger

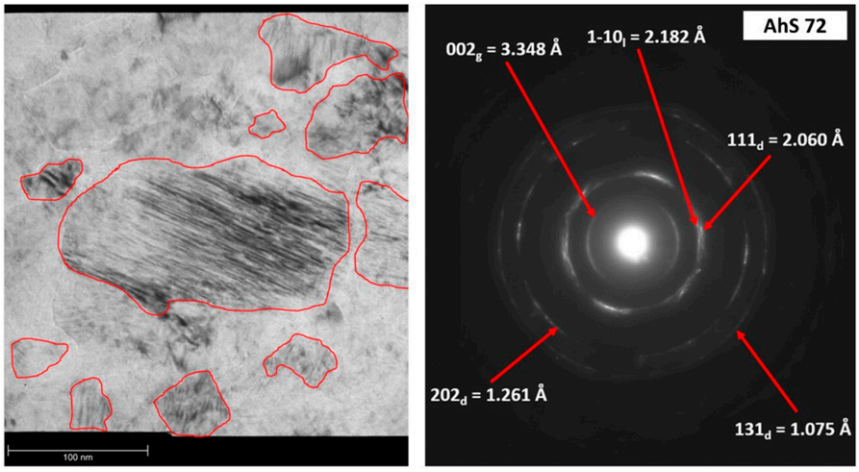

Fig. 3. (*Left*) A typical bright-field image of the AhS 72 sample, which shows diamond domains with size ranging from 20 to 150 nm. The corresponding electron diffraction image (*Right*) indicates that nanodiamonds are associated with graphite (see the ring at about 3.35 Å) and diamond with stacking faults, that is, lonsdaleite (see ring at about 2.18 Å), confirming the XRD results. The diffraction line indicators are represented by the (hkl) planes of diamond (indicated with the subscript "d") and graphite (indicated with the subscript "g") and give the spacing in angstroms. These images were obtained with a Philips CM200 transmission electron microscope.

diamonds within these blade-shaped regions, parallel to the long dimension of the laths which likely represents the trace of (0001) in original graphite (23, 24), strongly suggests that the diamonds are pseudomorphing original graphite crystals and formed in a rapid process that did not allow time for external graphite morphology to be replaced by diamond morphology. In fact, diamonds pseudomorphing original graphite forms is what is observed for diamonds formed in the Popigai impact crater (49, 50) in which aggregates of submicron-sized diamonds show external tabular shapes preserving the crystal habit of precursor graphite flakes (though we note that the primary graphite morphologies inferred for ureilites differ from those at Popigai).

As emphasized above, our observations of NWA 7983 represent an astonishing intimate association of micro- and nanodiamonds reported in a natural sample. The nanodiamond aggregates in NWA 7983 are especially abundant and render this ureilite even more resistant to cutting and polishing than most ureilites, similar to industrially produced ultrahard nanodiamonds (51, 52). As discussed by refs. 44–46, nanodiamonds of this type are the typical product of shock compression of disordered graphite, and nanodiamonds in ureilites and other meteorites are widely interpreted to be the product of impact shock (1, 4, 53, 54).

However, the formation mechanism of the large diamonds observed in NWA 7983, and the question of whether they formed at the same time as the nanodiamonds, are the critical issues in this investigation, as refs. 12 and 13 argue that such large sizes require long growth times under static high-pressure conditions. Hezel et al. (3) reported diamonds up to 5 μm in size (identified by in situ XRD) in a ureilite, and based on their close association with compressed graphite and secondary, polycrystalline graphite argued for formation of the diamonds by shock. The diamonds observed in this work are even larger and may require additional evidence to support formation in a shock event, the principal objections being the extremely short duration of peak pressure conditions during a shock event (45, 51, 55) and the kinetic/energetic limitations associated with direct transformation from graphite (45). We address both of these issues.

First, although the effective duration of a typical laboratory shock experiment is on the order of a microsecond, and so does not allow time for the growth of diamonds beyond very small (less than micrometer) sizes (46), large natural impacts have a significantly longer duration of high-pressure conditions (45). The largest craters on asteroid 4 Vesta, with a diameter of 400 to 500 km, could have formed from a 25- to 30-km impactor, with peak shock pressure during the compression stage lasting for 4 to 5 s (56). During the major impact event of UPB disruption, which is the most likely event in the history of ureilites to explain the majority of their shock features (17, 21, 32), the duration of the compression stage could have been comparably long, based on the impact parameters of ref. 57 for catastrophic disruption of the UPB and equations of ref. 56.

Second, although the direct transformation of graphite to diamond may require higher pressures and/or longer duration of pressure than those of many shock events (44, 45, 58) the catalyzed formation of diamonds in metallic (Fe,Ni,Co)-C melts proceeds at notably lower pressures and higher reaction rates and has long been used in industrial production of diamonds (59–64). Catalysis by metallic melts (referred to as the solvent method or solvent-catalysis in some literature) is likely to have been a significant factor in formation of diamonds in ureilites. As shown in *SI Appendix*, Fig. S1, the millimeter-sized euhedral graphite crystals in ureilites of very low shock level are intimately associated with Fe,Ni metal. Such metal is a common interstitial component associated with carbon in most ureilites (18, 65). Goodrich et al. (65) argued that the metal in ureilites represents Fe-Ni-C melt that was present at $T \geq 1{,}150$ °C and remained after extraction of lower-temperature Fe,S-enriched melt during the igneous stage of ureilite formation. The presence in ureilite silicates of ∼5- to 150-μm-diameter metallic spherules, consisting of cohenite (Fe_3C), metal, schreibersite (Fe_3P), and sulfide, constitute direct evidence for the presence of such melts at magmatic temperatures (65, 66). The impact disruption of the UPB occurred while the silicates were still hot, ∼1,050 ± 50 °C (18, 21). The temperature increase associated with this impact shock event, assuming a 5 $km \cdot s^{-1}$ relative velocity, would have been on the order of 200 to 300 °C (67). Thus, grain boundary metal would have been remelted to create Fe-Ni-C liquids, and it seems inescapable that they would have had a large effect on the growth rate of diamonds forming during the shock event. The importance of such metallic liquids in catalyzing the formation of diamonds from graphite in ureilites was previously suggested by ref. 6 though not discussed for diamonds of such large sizes as those observed here.

There is, in fact, a vast literature on the formation of diamonds via the catalytic method, because of the industrial importance of diamond. In general, the catalyzed formation of diamonds from graphite occurs in a very thin film of molten metal in contact with graphite (62, 64, 68), with reported diamond growth rates ranging from 0.2 to 0.4 μm/s at 5.4 GPa and 1,127 °C (62) to 30 to 60 μm/s (in the first 20 s) at 4.5 GPa and 1,100 to 1,200 °C (59). The latter rates would easily permit formation of a 100-μm-sized diamond, as observed in NWA 7983, in the ∼4 to 5 s estimate made above for the duration of peak pressure during the catastrophic disruption of the UPB. This evidence is sufficient to show that formation of large diamonds in ureilites during shock events is plausible and to cast reasonable doubt on the necessity for much longer growth times under static high-pressure conditions (12, 13).

Catalyzed formation of diamonds during a shock event can also account for simultaneous formation of micro- and nanodiamonds in ureilites. For example, using a technique of pulsed heating of a graphite-metal experimental charge in a static high-pressure apparatus at 8 to 14 GPa, which simulates natural impact processes (45, 55) with respect to duration of peak pressures and temperatures, Varfolomeeva (60) reported formation of up to 10-μm-sized diamonds near the catalyst and nanodiamonds in other parts of the experimental charge (*SI Appendix*, Fig. S14).

Catalysis of diamond formation from graphite via metallic melts may also explain other features of the diamonds in NWA 7983. For example, we hypothesize that the striped internal textures of the carbon areas, defined by stripes of concentrated (higher abundance of larger) diamonds and C-dominated (Fe,S-absent) chemistry (darker in BEI) alternating with stripes of dominantly nanodiamonds and C+Fe+S chemistry, could have formed if the metallic melts were injected between (0001) graphite platelets [assuming the long dimensions of the carbon masses to represent the trace of (0001) in original large graphite crystals]. Growth of larger diamonds then proceeded to form the largely Fe-free dark stripes adjacent to the metallic liquids, while the lighter stripes retain concentrations of residual Fe intermixed with nanodiamonds. In addition, ref. 59 suggested that the growth of diamonds from metallic liquids proceeded through the intermediate step of carbide formation, which could explain the association of cohenite (Fe_3C) with diamonds observed in this work (Fig. 2*C*). Another type of inclusion, chromite, reported by ref. 13 in ureilite diamonds, could also support catalytic formation of diamonds during a shock event. Nabiei et al. (13) noted that the nearly pure (Al-Ti-Mg-free) compositions of the chromite required crystallization from metallic melts (references 22 and 23 in ref. 13). We agree with this interpretation, which is strongly supported by the presence of similarly pure chromite in the metallic metal–cohenite–sulfide–phosphide spherules in ureilite silicates mentioned above (65, 66). However, in contrast to Nabiei et al. (13), who argued that the presence of such melts was inconsistent with the low-pressure igneous setting of ureilite

formation, we note that the metallic spherules provide direct evidence that such melts were present in the primary ureilite silicate assemblage (65, 66) and so could have been remobilized to catalyze the formation of diamonds in an impact shock event.

Additional Evaluation of Proposed Evidence for High Static Pressure. The 100-μm-sized single diamond crystal that we observed in NWA 7983 constitutes the first definite report of diamonds of this size in a ureilite. Nabiei et al. (13) did not determine the sizes of the diamonds they studied in MS-170 (e.g., no micro XRD was performed showing diffraction spots) but rather relied on the previous report by Miyahara et al. (12) of large diamonds in this sample. In fact, the "large" diamonds reported by Miyahara et al. (12) in MS-170 were not actually large single crystals but rather aggregates of many individual (unconnected) segments having almost the same crystallographic orientation. These aggregates were interpreted (12, 13) to have originally been large single crystals. However, this is not the only possible interpretation. In fact, an aggregate of similarly oriented small crystals is what is expected for diamonds formed by shock compression of oriented graphite (50, 69, 70), as noted also by ref. 6. Miyahara et al. (12) stated that they did not observe the predicted crystallographic relationship between diamond and graphite, and used this as an argument against a shock origin. However, if originally large single graphite crystals had been internally recrystallized in a shock event to nanometric, randomly oriented grains (like those observed in the samples studied here), which is likely (71), their current orientations relative to the diamond are irrelevant. Instead, the orientation of the diamonds would have to be compared with the original orientation of the graphite precursors.

By contrast, the presence of a truly single-crystal 100-μm-sized diamond in a highly shocked ureilite (NWA 7983) makes it more likely that such diamonds actually formed as a result of the shock process, rather than just having survived it. The shock state of silicates in MS-170 was not investigated by refs. 12 and 13 but was classified as S3 by ref. 31, which implies shock pressures of 5 to 10 GPa (47), sufficient to produce diamonds (see ref. 6). Critically, the external morphologies of the carbon masses in MS-170 are no different from those in NWA 7983 or other ureilites—that is, they are elongated masses along silicate grain boundaries, suggesting that they were originally large, single crystals of graphite, as discussed above for all ureilites. This can be observed from inspection of figure 1 of ref. 13 compared with *SI Appendix*, Fig. S1 and was confirmed by recent studies of our own on MS-170. This makes it extremely unlikely that the diamonds formed during long residence times at high pressures, because if they had then external diamond morphologies would have formed. In other words, there is no evidence that MS-170 is an unusual ureilite preserving diamonds formed in a planetary mantle.

Finally, Miyahara et al. (12) also reported the observation of sector zoning of nitrogen in diamond assemblages in MS-170 and argued that this required "sluggish growth" as in a static high-pressure setting. However, the evidence they present for sector zoning (e.g., figure 5 of ref. 12) is at best ambiguous. Heterogeneous nitrogen distribution is clearly shown, but its relationship to diamond crystal morphology is unclear, given that the diamond consists of several unconnected segments separated by areas of graphite (as discussed above) and no crystal orientation information is given. Furthermore, even if sector zoning of nitrogen is present in large ureilite diamonds, this would not require long, slow growth. For example, diamonds grown by the DeBeers Diamond Research Laboratory using an Fe-Ni metal catalyst for diamond growth developed strong sector zonation of nitrogen in 15 to 20 s (*SI Appendix*, Fig. S15), which is hardly "sluggish." The distribution of nitrogen in large ureilite diamonds, and what it implies for their formation, warrants further investigation, but at this time there is no evidence that it supports a high static pressure.

Conclusions

In conclusion, the results from combined micro XRD, TEM, SEM, EMPA, and micro-Raman spectroscopy of three highly shocked ureilites suggest that the most likely process by which both microdiamonds and nanodiamonds in ureilites formed is in a shock event characterized by a peak pressure possibly as low as 15 GPa, the shock level recorded by the silicates. Micrometer-sized diamonds can form from crystalline graphite in shock events when catalyzed by metallic Fe-Ni-C liquid, which was demonstrably present during the major shock events that occurred on the UPB, and do not require high static pressures and long growth times. None of the minor Fe-S-P phases associated with the diamonds in ureilites require high static pressures either, nor does sector zonation of nitrogen in diamonds. We find no compelling evidence that diamonds in ureilites formed in large planetary bodies or planetary embryos (13).

Methods

Petrological and mineralogical features of silicate and carbon phases in ureilites AhS 209b, AhS 72, and NWA 7983 were studied in polished sections by optical microscopy and electron microscopy (SEM) at the Lunar and Planetary Institute (Universities Space Research Association, Houston, TX), the ARES division at NASA, JSC, and the University of Padova. Carbon phases were additionally studied by XRD at the University of Padova, synchrotron-radiation X-ray microdiffraction at the Paul Scherrer Institute, TEM at Goethe University in Frankfurt, and micro-Raman spectroscopy at JSC. Contamination of the samples by diamond from the cutting and polishing was avoided by polishing the samples with silicon carbide paper. Further details of the techniques used in this work are provided in *SI Appendix*.

Data Availability. All study data are included in the paper, *SI Appendix*, and Datasets S1–S3. The three diffractograms for AhS 209b, AhS 72, and NWA 7983 Diamond 2 are available in a .txt format (intensity vs. 2θ angle) and can be visualized using any graphical software (Datasets S1–S3).

ACKNOWLEDGMENTS. We thank Marco van Gemeren for sample preparation and Kent Ross for assistance with SEM/EMPA. We are grateful to James Van Orman, Allan Treiman, and Maurizio Bellotto for helpful discussions. This work was supported by Programma Nazionale di Ricerche in Antartide (PNRA) 2018 grant PNRA18 00247–A to F. N. and NASA grants 80NSSC17K0165, NNX17AH09GS03, and 80NSSC19K0507 to C.A.G. M.M., A.B., M.C. Domeneghetti, and M.A. were funded by the IMPACt project (R164WEJAHH); M.C. Domeneghetti was funded by the PNRA 2016 to L. Folco. This is Lunar and Planetary Institute (LPI) contribution 2393. LPI is operated by USRA under a cooperative agreement with the Science Mission Directorate of NASA.

1. M. E. Lipschutz, Origin of diamonds in the ureilites. *Science* **143**, 1431–1434 (1964).
2. Y. Nakamuta, Y. Aoiko, Mineralogical evidence for the origin of diamond in ureilites. *Meteorit. Planet. Sci.* **35**, 487–493 (2000).
3. D. C. Hezel *et al.*, In situ micro-Raman and X-ray diffraction study of diamonds and petrology of the new ureilite UAE 001 from the United Arab Emirates. *Meteorit. Planet. Sci.* **43**, 1127–1136 (2008).
4. C. Le Guillou, J. N. Rouzaud, L. Remusat, A. Jambon, M. Bourot-Denise, Structures, origin and evolution of various carbon phases in the ureilite Northwest Africa 4742 compared with laboratory-shocked graphite. *Geochim. Cosmochim. Acta* **74**, 4167–4185 (2010).
5. A. J. Ross *et al.*, MicroRaman spectroscopy of diamond and graphite in Almahata Sitta and comparison with other ureilites. *Meteorit. Planet. Sci.* **46**, 364–378 (2011).
6. Y. Nakamuta, F. Kitajima, K. Shimada, In situ observation, X–ray diffraction and Raman analyses of carbon minerals in ureilites: Origin and formation mechanisms of diamond in ureilites. *J. Mineral. Petrol. Sci.* **111**, 252–269 (2016).
7. C. A. Lorenz, A. A. Shiryaev, I. I. Vlasov, S. E. Borisovsky, Metamorphism of four desert ureilites and luminescence spectroscopy of defects in ureilitic diamonds. *Meteorit. Planet. Sci.* **54**, 1197–1214 (2019).
8. K. Fukunaga, J. Matsuda, K. Nagao, M. Miyamoto, K. Ito, Noble-gas enrichment in vapour-growth diamonds and the origin of diamond in ureilites. *Nature* **328**, 141–143 (1987).
9. J. I. Matsuda, K. Fukunaga, K. Ito, Noble gas studies in vapor-growth diamonds: Comparison with shock produced diamonds and the origin of diamonds in ureilites. *Geochim. Cosmochim. Acta* **55**, 2011–2023 (1991).

10. J. I. Matsuda, A. Kusumi, H. Yajima, Y. Syono, Noble gas studies in diamonds synthesized by shock loading in the laboratory and their implications on the origin of diamonds in ureilites. *Geochim. Cosmochim. Acta* **59**, 4939–4949 (1995).
11. H. C. Urey, Diamonds, meteorites, and the origin of the solar system. *Astrophys. J.* **124**, 623–637 (1956).
12. M. Miyahara *et al*., Unique large diamonds in a ureilite from Almahata Sitta 2008 TC_3 asteroid. *Geochim. Cosmochim. Acta* **163**, 14–26 (2015).
13. F. Nabiei *et al*., A large planetary body inferred from diamond inclusions in a ureilite meteorite. *Nat. Commun.* **9**, 1327 (2018).
14. G. Vdovykin, Ureilites. *Space Sci. Rev.* **10**, 483–510 (1970).
15. J. L. Berkley, G. J. Taylor, K. Keil, G. E. Harlow, M. Prinz, The nature and origin of ureilites. *Geochim. Cosmochim. Acta* **44**, 1579–1597 (1980).
16. C. A. Goodrich, Invited review. Ureilites: A critical review. *Meteorit. Planet. Sci.* **352**, 327–352 (1992).
17. C. A. Goodrich, E. R. D. Scott, A. M. Fioretti, Ureilitic breccias: Clues to the petrologic structure and impact disruption of the ureilite parent body. *Chem. Erde* **64**, 283–327 (2004).
18. D. W. Mittlefehldt, T. J. McCoy, C. A. Goodrich, A. Kracher, Non-chondritic meteorites from asteroidal bodies. *Rev. Mineral. Geochem.* **36**, 4.1-4.195 (1998).
19. C. A. Goodrich *et al*., Origin and history of ureilitic material in the solar system: The view from asteroid 2008 TC_3 and the Almahata Sitta meteorite. *Meteorit. Planet. Sci.* **50**, 782–809 (2015).
20. H. Downes, D. W. Mittlefehldt, N. T. Kita, J. W. Valley, Evidence from polymict ureilites for a disrupted and re-accreted single ureilite parent asteroid gardened by several distinct impactors. *Geochim. Cosmochim. Acta* **72**, 4825–4844 (2008).
21. J. S. Herrin *et al*., Thermal and fragmentation history of ureilitic asteroids: Insights from the Almahata Sitta fall. *Meteorit. Planet. Sci.* **45**, 1789–1803 (2010).
22. E. A. Cloutis *et al*., Spectral reflectance properties of ureilites. *Meteorit. Planet. Sci.* **45**, 10–11 (2010).
23. J. L. Berkley, J. H. Jones, Primary igneous carbon in ureilites: Petrological implications. *J. Geophys. Res.* **87**, A353–A364 (1982).
24. A. H. Treiman, J. L. Berkley, Igneous petrology of the new ureilites Nova 001 and Nullarbor 010. *Meteoritics* **29**, 843–848 (1994).
25. J. F. Wacker, Noble gases in the diamond-free ureilite ALHA78019: The roles of shock and nebular processes. *Geochim. Cosmochim. Acta* **50**, 633–642 (1986).
26. M. Murri *et al*., Quantifying hexagonal stacking in diamond. *Sci. Rep.* **9**, 10334 (2019).
27. S. J. Desch, J. G. O'Rourke, L. K. Schaefer, T. G. Sharp, D. L. Schrader, Diamonds in ureilites from Mars. *Lunar Planet. Sci. Conf. Abstr* **50**, 1646 (2019).
28. A. Ruzicka, J. Grossman, A. Bouvier, D. K. Herd, B. Agee, The Meteoritical Bulletin, No. 102. *Meteorit. Planet. Sci.* **50**, 1662 (2015).
29. P. Jenniskens *et al*., The impact and recovery of asteroid 2008 $TC_{(3)}$. *Nature* **458**, 485–488 (2009).
30. M. H. Shaddad *et al*., The recovery of asteroid 2008 TC_3. *Meteorit. Planet. Sci.* **45**, 1557–1589 (2010).
31. M. Horstmann, A. Bischoff, The Almahata Sitta polymict breccia and the late accretion of asteroid 2008 TC_3. *Chem. Erde* **74**, 149–183 (2014).
32. P. H. Warren, A. E. Rubin, Pyroxene-selective impact smelting in ureilites. *Geochim. Cosmochim. Acta* **74**, 5109–5133 (2010).
33. J. L. Berkley, Four Antarctic ureilites: Petrology and observations on ureilite petrogenesis. *Meteoritics* **21**, 169–189 (1981).
34. R. Delhez, E. J. Mittemeijer, Determination of crystallite size and lattice distortions through X-ray diffraction line profile analysis. *Anal. Chem.* **312**, 1–16 (1982).
35. M. Leoni, F. Gualtieri, N. Roveri, Simultaneous refinement of structure and microstructure of layered materials. *J. Appl. Cristallogr.* **37**, 166–173 (2004).
36. V. I. Korepanov, H. Witek, H. Okajima, E. Ōsawa, H. O. Hamaguchi, Communication: Three-dimensional model for phonon confinement in small particles: Quantitative bandshape analysis of size-dependent Raman spectra of nanodiamonds. *J. Chem. Phys.* **140**, 041107 (2014).
37. S. A. Solin, A. K. Ramdas, Raman spectrum of diamond. *Phys. Rev. B* **1**, 1687–1698 (1970).
38. S. Osswald, V. N. Mochalin, M. Havel, G. Yushin, Y. Gogotsi, Phonon confinement effects in the Raman spectrum of nanodiamond. *Phys. Rev. B* **80**, 75419 (2009).
39. A. C. Ferrari, J. Robertson, Raman spectroscopy of amorphous, nanostructured, diamond-like carbon, and nanodiamond. *Philos. Trans. A Math. Phys. Eng. Sci.* **362**, 2477–2512 (2004).
40. D. A. Minin, A. Shatskiy, K. D. Litasov, H. Ohfuji, The Fe–Fe_2P phase diagram at 6 GPa. *High Pressure Res.* **39**, 50–68 (2019).
41. A. J. Stewart, M. W. Schmidt, Sulfur and phosphorus in the Earth's core : The Fe-P-S system at 23 GPa. *Geophys. Res. Lett.* **34**, 5–9 (2007).
42. K. Righter, N. L. Chabot, Moderately and slightly siderophile element constraints on the depth and extent of melting in early Mars. *Meteorit. Planet. Sci.* **176**, 157–176 (2011).
43. K. D. Litasov, S. N. Teplyakova, A. Shatskiy, K. E. Kuper, Fe-Ni-P-S melt pockets in Elga IIE iron meteorite: Evidence for the origin at high-pressures up to 20 GPa. *Minerals* **9**, 616 (2019).
44. P. S. De Carli, Shock wave synthesis of diamond and other phases. *MRS Proc.* **383**, 21–31 (1995).
45. P. S. De Carli *et al*., "Laboratory impact experiments versus natural impact events" in *Catastrophic Events and Mass Extinctions: Impacts and Beyond*, C. Koeberl, K. G. MacLeod, Eds. (GSA Special Paper, Geological Society of America, Boulder, CO, 2002), Vol. 356, pp. 595–605.
46. P. S. Decarli, J. C. Jamieson, Formation of diamond by explosive shock. *Science* **133**, 1821–1822 (1961).
47. D. Stöffler, C. Hamann, K. Metzler, Invited Review, Shock metamorphism of planetary silicate rocks and sediments: Proposal for an updated classification system. *Meteorit. Planet. Sci.* **49**, 5–49 (2018).
48. F. Nestola *et al*., $CaSiO_3$ perovskite in diamond indicates the recycling of oceanic crust into the lower mantle. *Nature* **555**, 237–241 (2018).
49. C. Koeberl *et al*., Diamonds from the Popigai impact structure, Russia. *Geology* **25**, 967–970 (1997).
50. H. Ohfuji *et al*., Natural occurrence of pure nano-polycrystalline diamond from impact crater. *Sci. Rep.* **5**, 14702 (2015).
51. T. Irifune, A. Kurio, S. Sakamoto, T. Inoue, H. Sumiya, Materials: Ultrahard polycrystalline diamond from graphite. *Nature* **421**, 599–600 (2003). Correction in: *Nature* **421**, 806 (2003).
52. F. Isobe, H. Ohfuji, H. Sumiya, T. Irifune, Nanolayered diamond sintered compact obtained by direct conversion from highly oriented graphite under high pressure and high temperature. *J. Nanomater.* **2013**, 380165 (2013).
53. L. A. J. Garvie, P. Németh, P. R. Buseck, Transformation of graphite to diamond via a topotactic mechanism. *Am. Mineral.* **99**, 531–538 (2014).
54. S. Mostefaoui, A. El Goresy, P. Hoppe, Ph. Gillet, U. Ott, Mode of occurrence, textural settings and nitrogen-isotopic compositions of in situ diamonds and other carbon phases in the Bencubbin meteorite. *Earth Planet. Sci. Lett.* **204**, 89–100 (2002).
55. F. P. Bundy, J. S. Kasper, Hexagonal diamond–A new form of carbon. *J. Chem. Phys.* **46**, 3437–3446 (1967).
56. P. Gillet, A. El Goresy, Shock events in the solar system: The message from minerals in terrestrial planets and asteroids. *Annu. Rev. Earth Planet. Sci.* **41**, 257–285 (2013).
57. P. Michel *et al*., Selective sampling during catastrophic disruption: Mapping the location of reaccumulated fragments in the original parent body. Proceedings of the 8th Catastrophic Disruption Workshop. *Planet. Space Sci.* **107**, 24–28 (2015).
58. C. Le Guillou, F. Brunet, T. Irifune, H. Ohfuji, J.-N. Rouzaud, Nanodiamond nucleation below 2273 K at 15 GPa from carbons with different structural organizations. *Carbon* **45**, 636–648 (2007).
59. G. N. Bezrukov *et al*., "Kinetic features of diamond crystallization" in *Growth of Crystals*, N. N. Sheftal', E. I. Givargizov, Eds. (Consultants Bureau, New York,, 1975), Vol. 9, pp. 74–77.
60. T. D. Varfolomeeva, "Synthesis and investigation of polycrystalline diamond," PhD thesis, Institute for High Pressure Physics, USSR Academy of Sciences (1971), p. 154.
61. L. F. Trueb, An electron-microscope study of shock-synthesized diamond. *J. Appl. Phys.* **39**, 4707–4716 (1968).
62. H. M. Strong, R. E. Hanneman, Crystallization of diamond and graphite. *J. Chem. Phys.* **45**, 3668–3676 (1967).
63. I. I. Fedorov, A. A. Chepurov, J. M. Dereppe, Redox conditions of metal-carbon melts and natural diamond genesis. *Geochem. J.* **36**, 247–253 (2002).
64. F. P. Bundy *et al*., The pressure-temperature phase and transformation diagram for carbon; updated through 1994. *Carbon* **34**, 141–153 (1996).
65. C. A. Goodrich, R. D. Ash, J. A. Van Orman, K. Domanik, W. F. McDonough, Metallic phases and siderophile elements in main group ureilites: Implications for ureilite petrogenesis. *Geochim. Cosmochim. Acta* **112**, 340–373 (2013).
66. C. A. Goodrich, J. L. Berkley, Primary magmatic carbon in ureilites: Evidence from cohenite-bearing metallic spherules. *Geochim. Cosmochim. Acta* **50**, 681–691 (1986).
67. D. Stöffler, E. R. D. Klaus Keil, Scott, Shock metamorphism of ordinary chondrites. *Geochim. Cosmochim. Acta* **55**, 3845–3867 (1991).
68. H. P. Bovenkerk, F. P. Bundy, H. M. Strong, R. H. Wentorf Jr., H. T. Hall, Preparation of diamond. *Nature* **184**, 1094–1098 (1959).
69. D. J. Erskine, W. J. Nellis, Shock-induced martensitic phase transformation of oriented graphite to diamond. *Nature* **349**, 317–319 (1991).
70. H. Ohfuji, M. Nakaya, A. P. Yelisseyev, V. P. Afanasiev, K. D. Litasov, Mineralogical and crystallographic features of polycrystalline yakutite diamond. *J. Mineral. Petrol. Sci.* **112**, 46–51 (2017).
71. A. N. Dremin, O. N. Breusov, "Dynamic synthesis of superhard materials" in *Shock Waves in Materials Science*, A. B. Sawaoka, Ed. (Springer, Tokyo, 1993), pp. 17–34.